

Numerical simulation of laminar flow past a circular cylinder

B.N. Rajani^a, A. Kandasamy^b, Sekhar Majumdar^{a,*}

^a CTFD Division, National Aerospace Laboratories, Airport Road, Bangalore 560 017, India

^b Department of Mathematical and Computational Sciences, National Institute of Technology, Karnataka, Surathkal 575 025, India

Received 23 January 2007; received in revised form 14 January 2008; accepted 18 January 2008

Available online 2 February 2008

Abstract

The present paper focuses on the analysis of two- and three-dimensional flow past a circular cylinder in different laminar flow regimes. In this simulation, an implicit pressure-based finite volume method is used for time-accurate computation of incompressible flow using second order accurate convective flux discretisation schemes. The computation results are validated against measurement data for mean surface pressure, skin friction coefficients, the size and strength of the recirculating wake for the steady flow regime and also for the Strouhal frequency of vortex shedding and the mean and RMS amplitude of the fluctuating aerodynamic coefficients for the unsteady periodic flow regime. The complex three dimensional flow structure of the cylinder wake is also reasonably captured by the present prediction procedure.

© 2008 Elsevier Inc. All rights reserved.

Keywords: Laminar flow; Circular cylinder; Vortex shedding; Unsteady RANS procedure; Implicit finite volume method; Three-dimensional flow

1. Introduction

In spite of extensive experimental and numerical studies almost over a century, flow around a circular cylinder still remains a challenging problem in fluid mechanics, where intensive investigations are continued even today to understand the complex unsteady dynamics of the cylinder wake flow. Cross-flow normal to the axis of a stationary circular cylinder and the associated problems of heat and mass transport are encountered in a wide variety of engineering applications. Both experimental measurements and numerical computations have confirmed the onset of instability of the wake flow behind a cylinder beyond a critical Reynolds number, leading finally to a kind of periodic flow identified by definite frequencies, well-known in the literature as the Von Karman vortex street. In case of laminar flow past cylinders with regular polygonal cross-section, the flow usually separates at one or more sharp corners of the cross-section geometry itself, forming a system of vortices in the wake on either side of the mid symmetry plane. On the other hand, for a circular cylinder, where the point of flow separation is decided by the nature of the upstream boundary layer, the physics of the flow is much more complex than what its relatively simple shape might suggest.

* Corresponding author. Tel.: +91 80 25051619/25051616; fax: +91 80 25220952.

E-mail addresses: rajani@ctfd.cmmacs.ernet.in (B.N. Rajani), sekhar@ctfd.cmmacs.ernet.in (S. Majumdar).

As the flow Reynolds number ($Re = UD/\nu$) based on the free stream velocity (U), cylinder diameter (D) and kinematic viscosity ν of the fluid, changes from a creeping laminar flow value of the order of 0.1 to a turbulent flow of the Re of a million or even higher, variety of physical complexities start taking place. Steady laminar flow exists at Reynolds number between 5 and 40 with a pair of symmetric counter-rotating vortices formed behind the cylinder. Beyond a critical value of Re , depending on the other flow disturbances, a transverse oscillation sets in with loss of flow symmetry and vortices are shed from the cylinder surface. Between $Re = 190$ and 260, wakes of two dimensional cylinders are observed to become susceptible to a primary instability mechanism which leads to the amplification of three dimensional disturbances and eventually to the development of strong streamwise oriented vortical structures. These three-dimensional disturbances alter the structure and evolution of the wake vortices and as a result, even at low Reynolds number, two-dimensional simulations often fail to accurately predict even gross flow quantities like mean drag coefficient and root mean square (RMS) of the lift fluctuation.

2. Characteristic regimes of flow past a circular cylinder

Recently Zdravkovich [1], in an excellent monograph, has compiled almost all the experimental, analytical and numerical simulation data on flow past cylinders, available since 1938 and systematically classified this challenging flow phenomenon into five different flow regimes based on the Reynolds number. In the present study, the computation is restricted only to the first few regimes designated by Zdravkovich as (1) creeping laminar state (L1) of flow ($0 < Re < 4$), (2) laminar flow (L2) with steady separation ($4 < Re < 48$) forming a symmetric contra-rotating pair of vortices in the near wake, (3) laminar flow (L3) with periodic vortex shedding ($48 < Re < 180$) and finally (4) part of the transition-in-wake (TrW) regime ($180 < Re < 400$) when the three-dimensional instabilities lead to the formation of streamwise vortex structure. Computations are carried out in the present work in the range of $0.1 < Re < 400$ for comparison with available measurement data or other computation results for both steady and unsteady flow situations. All the computations use an implicit pressure-based finite volume Navier–Stokes algorithm (RANS3D) for time-accurate prediction of the flow. This flow solution algorithm, originally proposed by the last author [2], has been further developed [3–5] at the CTFD Division, NAL, Bangalore during the last 10 years. The whole flow domain covering the L1–TrW regimes has first been computed under the assumption of two-dimensional flow. Later, in order to understand the effect of the three-dimensional disturbances on the complex wake vortex dynamics, three-dimensional analysis have been carried out at five different Reynolds number covering part of the L3 and TrW regimes, already reported in unclassified literature by a few researchers [6–9]. The present computation results have been compared to available measurement data and/or other computation results for the wake flow structures, the temporal evolution of drag coefficient, the variation of separation angle, stagnation pressure and base pressure behind the cylinder as the Reynolds number increases and also for the frequency and amplitude of the fluctuating forces arising out of the phenomenon of vortex shedding in the relevant flow regime.

3. Numerical simulation methodology

3.1. Governing equation

The Navier–Stokes equations for unsteady laminar incompressible flow may be written in a compact form in non-orthogonal curvilinear coordinates used in the present simulation as follows:

Momentum transport for the cartesian velocity component U_i :

$$\frac{\partial(\rho U_i)}{\partial t} + \frac{1}{J} \frac{\partial}{\partial x_j} \left[(\rho U_i U_k \beta_i^j) - \frac{\mu}{J} \left(\frac{\partial U_i}{\partial x_m} \beta_m^j + \frac{\partial U_k}{\partial x_m} \beta_i^m \beta_k^j \right) + P \beta_i^j \right] = S_{U_i}, \quad (1)$$

where J is the transformation Jacobian between cartesian and the curvilinear coordinates, β_j^i and β_i^j are the relevant metric coefficients related to the geometrical transformation, P is the pressure and j , k and m are used as repeated summing indices along the grid directions. U_i is the mean cartesian velocity solved for along the ' i -th' direction. These three momentum equations are further supplemented by the continuity equation as follows:

Mass conservation (continuity):

$$\frac{\partial}{\partial x_j} (\rho U_k \beta_k^j) = 0. \quad (2)$$

3.2. Finite volume formulation

The present flow solution algorithm (RANS3D) is an iterative two-step predictor–corrector procedure similar to the SIMPLE algorithm of Patankar [10]. In the predictor step, the momentum equations are solved to advance the velocity field partially in time for a guessed pressure field. The continuity is then ensured by solving a Poisson equation for pressure correction, followed by relevant correction of the pressure and velocity field in the corrector step. Integration of the momentum transport equations (Eq. (1)) over each control volume transforms the relevant pde's in the form of discrete algebraic equations representing a balance between the convective and diffusive fluxes through the cell faces and the other remaining terms as volume sources. Second order accurate central difference scheme is used for spatial discretisation of the convective and diffusive fluxes at the cell faces. The temporal derivatives are also discretised using the second order accurate three-level fully implicit scheme. The numerical stability is ensured by means of a deferred correction procedure [11], where a suitable weighting function is used to blend the flux from the desired scheme with upwind fluxes which allow some small numerical diffusion for stability of the solution. Using the relevant geometric factors with second order spatial and temporal discretisation schemes for the cell face fluxes and linearisation of the source terms, the flux balance equation is expressed in an implicit manner in the following quasilinear form:

$$\int \frac{\partial \phi}{\partial t} \Delta v + A_P \phi_P^{n+1} = \sum_{nb} A_{nb} \phi_{nb}^{n+1} + \text{SU}, \quad (3)$$

where $A_P = \sum A_{nb} - \text{SP}$; the coefficient A_{nb} represents the combined effect of convection and diffusion from the neighbouring nodes at the cell faces; SU and SP are the components of the linearised source term, Δv is the cell volume and Δt is the time step size. The superscripts of ϕ represent the respective time step. The detailed derivation of Eq. (3) in terms of the flow variables and the cell face projection areas is given elsewhere [3–5]. The Poisson equation for pressure correction representing the continuity is also transformed to a linearised equation for pressure correction in the form of Eq. (3). The corrections are added to the momentum-satisfying pressure and velocities, respectively, at the cell centers and cell faces. A segregated iterative method, coupled to the strongly implicit procedure of Stone [12], is used to solve the system of linear equations (Eq. (3)) corresponding to each transport equation in a sequential manner. At each time step the normalized residue for all the equations solved are brought down to a convergence criterion of 10^{-4} .

4. Results and discussion

The implicit finite volume solver RANS3D developed for general multiblock structured non-orthogonal grid, has been used in this work for both two- and three-dimensional computation of the problem. In case of L1 and L2 regime, where the flow is steady, the present computations are limited to two-dimensional flow only. Even in the L3 regime of periodic vortex shedding for Re up to 200, the flow structures in the periodic wake vortices are observed in measurement to be mostly two-dimensional, lying on a plane normal to the cylinder axis. The present computations up to $Re = 200$, are therefore carried out for two-dimensional flow only and the prediction results are compared to the measurement data reported in the literature for the Strouhal frequency, the circumferential variation of time-averaged surface pressure and skin friction and the mean and RMS values of the lift and drag coefficients. Beyond a critical range of Reynolds number of 180–200, the measurement as well as numerical simulation data demonstrate the susceptibility of the two-dimensional wake behind the cylinder to a three-dimensional Floquet instability mechanism [13] which amplifies the three-dimensional disturbances and eventually leads to the formation of strong streamwise-oriented vortex structure. Therefore in the present study, computations has been carried out for three-dimensional flow past a cylinder with a finite aspect ratio for Reynolds number varying from 100 to 400. The objective of this

three-dimensional flow computation is to test the accuracy of the RANS3D code for prediction of the integrated force coefficients and also to verify whether the characteristic three-dimensional features of this complex flow, observed in measurement or other computation reported in unclassified literature, could be captured by the present simulation.

4.1. Computational details

The two block radial polar grid and the boundary conditions used are shown in Fig. 1. Based on the earlier grid-sensitivity study by Rajani et al. [14], all the present calculations use 144 nodes stretched along the radial direction and 121 equispaced nodes around the circumferential direction. In case of three-dimensional flow situation, however, 32 equidistant parallel planes cover the total spanwise length of $2\pi D$ and periodic boundary conditions are used at the end planes. The wall normal distance of the first internal grid point is maintained at $\Delta r = 0.0001D$, required for adequate resolution of the sharp near wall gradients of the flow variables. The appropriate boundary conditions for the two blocks are shown in Fig. 1b. An impulsive start of the cylinder is simulated by specifying uniform inflow velocities ($U = U_{in}$ and $V = 0$) in the whole field except at the cylinder wall nodes, where no slip condition is imposed as initial conditions ($t = 0$) and maintained thereafter at all time instants ($t > 0$). Based on the earlier sensitivity studies [15], central difference scheme for convective flux discretisation coupled to second order accurate temporal discretisation with time step size $\Delta t = 0.05$ have been used for all the computations at different flow Reynolds number.

4.2. Creeping flow (L1) regime

Table 1 shows the computed values of the front ($\theta = 0^\circ$) stagnation pressure (C_{p0}), the base pressure (C_{pb}) at the back ($\theta = 180^\circ$) of the cylinder, and also the total drag coefficient (C_d) along with its pressure (C_{dp}) and friction (C_{df}) components at different Reynolds number varying from 0.1 to 6. The measurement of Taneda [16], Coutanceau and Bouard [17] and Homann [18] show that the flow separation on the cylinder surface starts at Reynolds number ranging from 5 to 7, depending on the blockage ratio λ (ratio of the cylinder diameter D and the tunnel diameter). However, for the present computation with no blockage, flow separation and formation of a closed wake is observed to take place only beyond $Re = 6.1$.

4.3. Steady closed wake flow (L2) regime

Measurement data show that for flow Reynolds number beyond approximately 5, the flow separates on the cylinder surface and the wake behind the cylinder consists of a pair of symmetric contra-rotating vortices on either side of the wake centreline. Further it was observed that as the flow Reynolds number increases, the

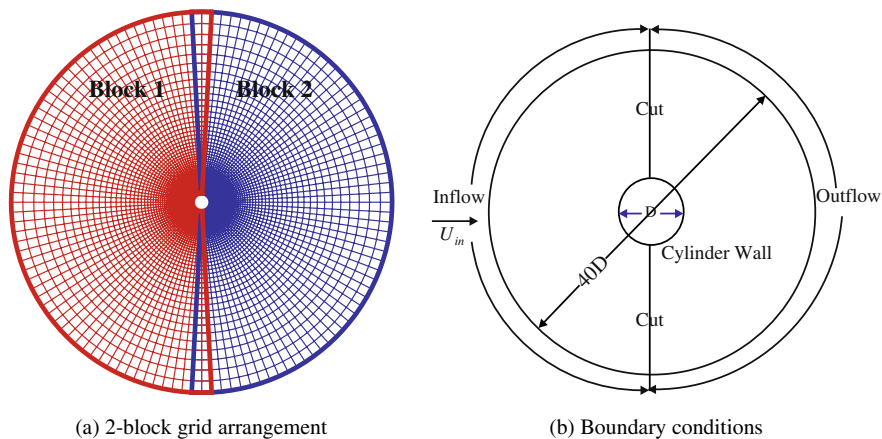


Fig. 1. Multiblock polar grid (124 × 144) and boundary conditions used for computation of flow past circular cylinder.

Table 1

Computed stagnation pressure, base pressure and drag coefficient for creeping flow past smooth cylinder

Re	C_{p0}	C_{pb}	C_{dp}	C_{df}	C_d
0.1	27.55	-28.33	43.94	43.82	87.76
0.4	8.05	-7.14	11.93	11.84	23.77
1.0	4.18	-3.15	5.74	5.61	11.35
1.6	3.17	-2.17	4.16	4.00	8.16
3.0	2.31	-1.39	2.85	2.63	5.48
3.9	2.05	-1.18	2.47	2.22	4.69
5.0	1.86	-1.02	2.17	1.90	4.07
6.0	1.74	-0.93	1.99	1.70	3.67

length of the closed wake (L_{wake}) increases (Fig. 2a) along with an upstream shifting of the flow separation point (θ_{sep}) on the cylinder surface (Fig. 5a). The computed variation of the wake length (L_{wake}) and the magnitude (U_{min}) of the maximum negative velocity inside the closed wake with the increase of the flow Reynolds number are shown in Fig. 2. Reasonably good agreement is observed between the present computation results and the measurement data of Coutanceau and Bouard [17] for the size and strength of the recirculation zone.

4.4. Laminar vortex shedding ($L3$) regime

The measurement data [1] show that beyond a critical Reynolds number of about 49, the steady closed near wake becomes unstable and a transverse oscillation starts near the end of the wake. As the Re is increased further, the vortices are shed alternately from the upper and lower cylinder surface at a definite frequency depending on the Reynolds number. Zdravkovich [1] has mentioned about the wide scatter of the reported values of this critical Reynolds number at which the near wake instability initiates even when the blockage is negligible. Norberg [19] has reported that this critical Reynolds number for the onset of vortex shedding is almost constant at $Re = 47.4$, but only for cylinders with aspect ratio larger than 40 this onset may be delayed as the aspect ratio decreases. Mittal [9] has concluded that the aspect ratio of the cylinder affects the onset of shedding as well as the occurrence of transition from one mode to the other mode of stability.

In order to determine the critical Reynolds number at which the cylinder wake with a symmetric vortex pair becomes unstable, the development of the transient lift coefficient, C_1 , derived from the present computation with double precision accuracy and a convergence criterion of 10^{-6} , has been analysed for $Re = 48, 49$ and 50 . In all the three cases shown in Fig. 3, the mean value of C_1 is very close to zero (of the order of 10^{-6}) as expected physically for the present flow situation. However, the transient variation of the peak amplitude

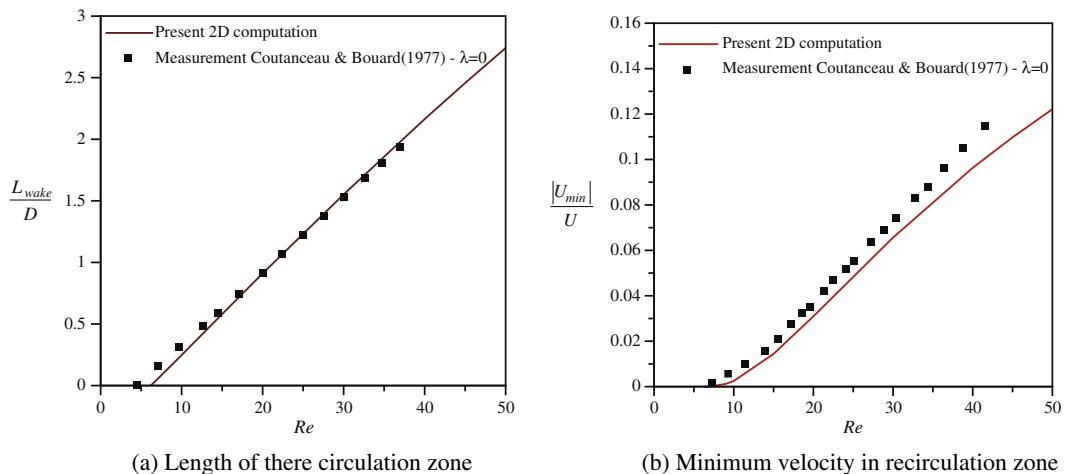


Fig. 2. Size and strength of the wake recirculation zone behind the cylinder.

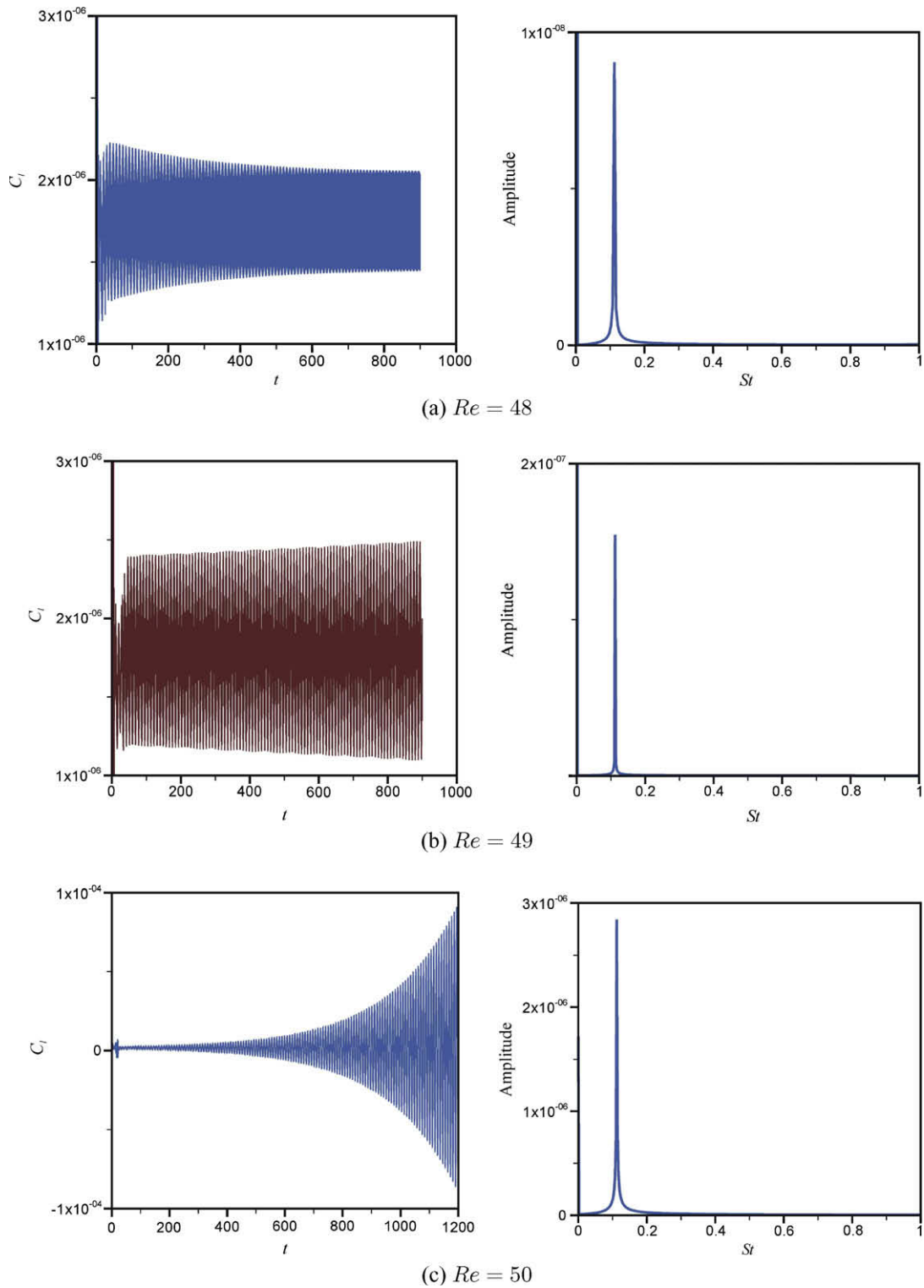


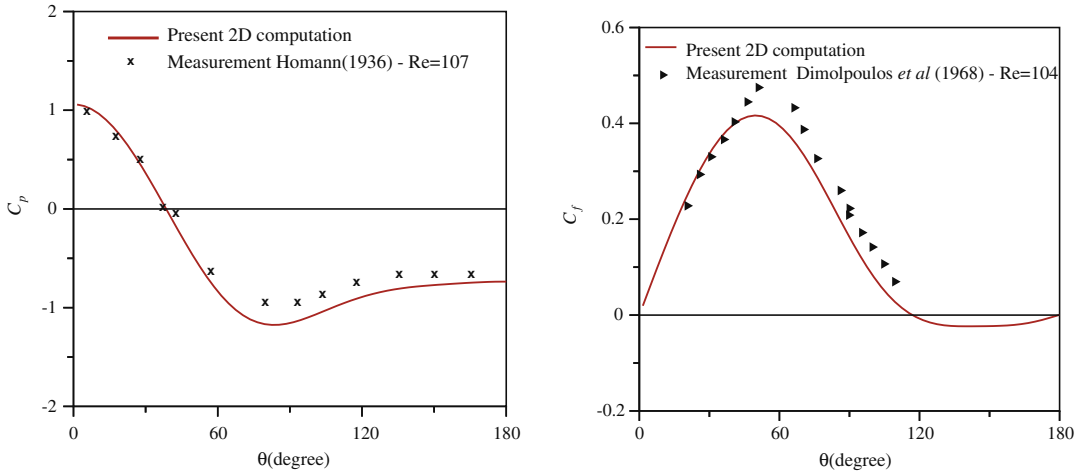
Fig. 3. Temporal variation of lift coefficient on time and frequency domain at different Reynolds number.

of C_1 is observed to be different for the three different Reynolds number cases investigated. At $Re = 48$, the maximum C_1 decays very slowly with time and is expected to reach a steady state after a long time, whereas

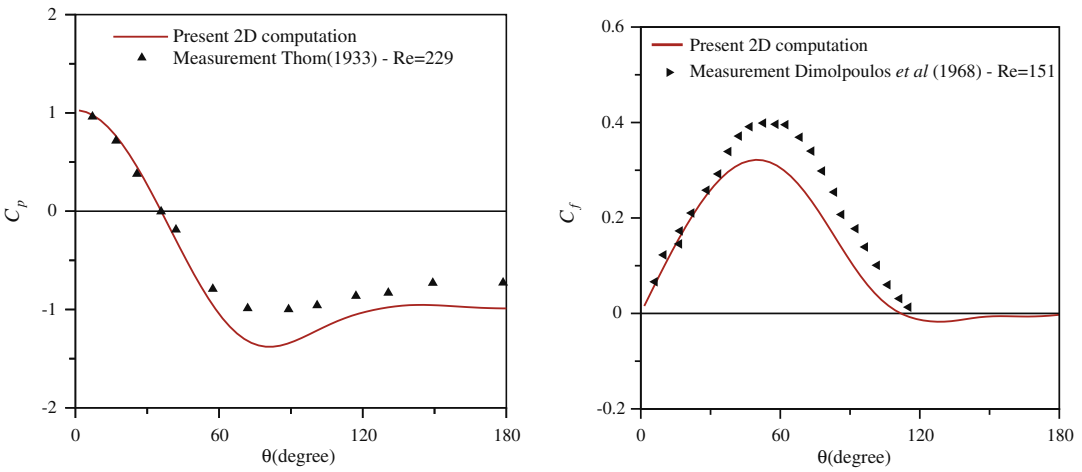
at $Re = 49$ the C_1 peaks appear to be growing very slowly with time, indicating perhaps that the periodicity is just set in and the wake is almost on the verge of losing its stable and steady structure. On the other hand at $Re = 50$, the peak C_1 value is observed to be growing at a very fast rate with time clearly indicating the unsteady or periodic state of the wake in an unambiguous manner. The corresponding variation of C_1 on frequency domain, derived from the Fast Fourier Transformation are shown in the same figure also indicates how the transient lift amplitude at a dominant frequency suddenly grows from the order of 10^{-8} at $Re = 48$ to an order of 10^{-6} at $Re = 50$. Based on this analysis one may conclude that for the present computation the critical Re must lie somewhere between $Re = 48$ and 49 and perhaps closer to $Re = 48$ only. It may be worthwhile to note that measurement data compiled by Zdravkovich [1] reports the critical Re for wake instability of a circular cylinder to be around 49 . Further in an accurate finite element computation of two-dimensional flow past a circular cylinder with infinite aspect ratio, Kumar and Mittal [20] have recently reported the critical Re to be 47.045 , based on similar argument of zero growth rate of the peak value of C_1 at the onset of the wake instability.

Two-dimensional flow computation has been carried out for different values of Re between 47 and 400 . When the statistically stationary state is indicated in the computation, the calculation is continued for the next 50 vortex shedding cycles and the time-averaged values are obtained by averaging the instantaneous field data on the flow variables for 50 shedding cycles. Available measurement data of Dimopoulos and Hanratty [21] on time-averaged surface pressure and skin friction coefficient have been compared to the corresponding computation results in Fig. 4. At all the Reynolds number, the agreement between the measurement data and the computational results is excellent in the accelerating flow zone covering the front part of the cylinder. But large discrepancies of the order of 20% or more are observed for the suction peak and the so-called base pressure in the rear part of the cylinder. This discrepancy may be attributed mainly to the inaccurate prediction of location of the unsteady flow separation point on the cylinder surface. At $Re = 200$ and 300 , the discrepancies may also be attributed partly to the three-dimensional instability of the wake along the spanwise direction, observed in experimental evidence. Even the blockage ratio (λ) which usually has a significant effect on the flow field, is also not clearly reported for the measurement conditions. Fig. 5 shows the time averaged separation angle, the stagnation pressure and base pressure over the whole range of Reynolds number ($0 < Re < 300$) for the two-dimensional flow analysis. For the separation angle, the agreement between the present prediction and the measurement data of Coutanceau and Bouard [17] at zero blockage ratio ($\lambda = 0$), is very good in the L2 regime. But beyond $Re = 49$, where the flow becomes unsteady, gross discrepancies are observed over the range of Re between 49 and 300 . At low Reynolds number ($Re < 200$), the discrepancies may be partly attributed to the blockage effect of the experimental situation; however, no definite trend of variation could be established. Over the whole range of Reynolds number, the computed mean stagnation pressure agrees reasonably well with the measurement data reported in literature [18,22]. In case of the base pressure, a kink is observed in both computation and measurement at the critical Reynolds number when the flow transforms from a steady to an unsteady or periodic situation. The agreement between computation and measurement data for the base pressure is reasonably good only up to about $Re = 150$, beyond which the three-dimensional instability plays an important role. The measurement data [23] shows two distinct kinks – one near $Re = 150$ and the other near $Re = 230$ indicating two different modes of the spanwise instability of the vortex system, whereas the two-dimensional computation shows simple monotonic reduction of the base pressure as the Reynolds number increases.

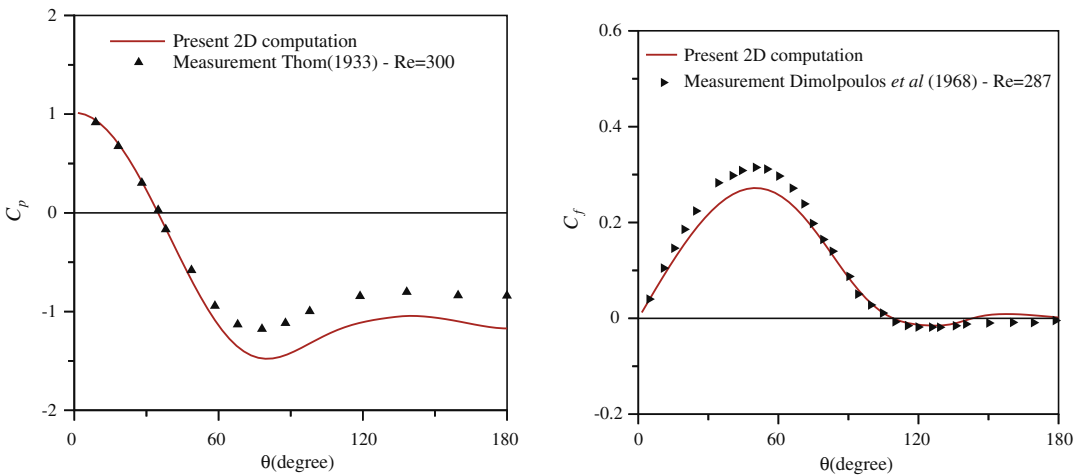
Some of the important variables of engineering interest for flow past cylinder with vortex shedding are the mean drag coefficient, and the Strouhal frequency of the lift coefficient. Fig. 6 shows the variation of mean drag coefficient – its pressure and friction components and the Strouhal number with varying flow Reynolds number. For the mean drag coefficient, kink is observed in the present computation result at critical Reynolds number of about 49 when vortex shedding starts. However, the overall agreement between the present computation and the compiled data of Zdravkovich [1] is reasonably good. In case of Strouhal frequency of the lift coefficient, the present computation agrees reasonably well with measurement data of Norberg [24] only up to about $Re = 150$ beyond which the two-dimensional flow computation overpredicts the Strouhal number. In order to investigate this matter further, three-dimensional flow computation has been carried out for Reynolds number ranging between 100 and 400 for which the results are discussed in the following section of this paper.



(a) $Re = 100$

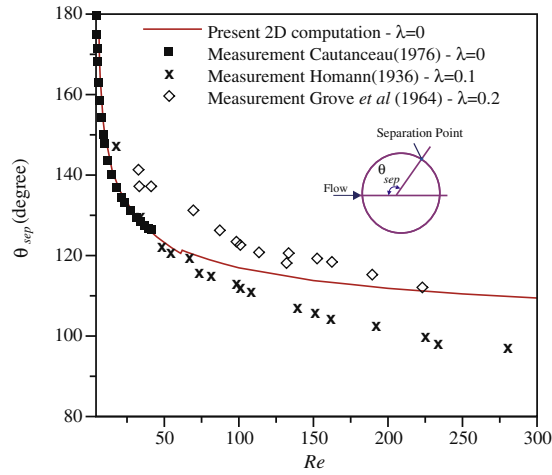


(b) $Re = 200$

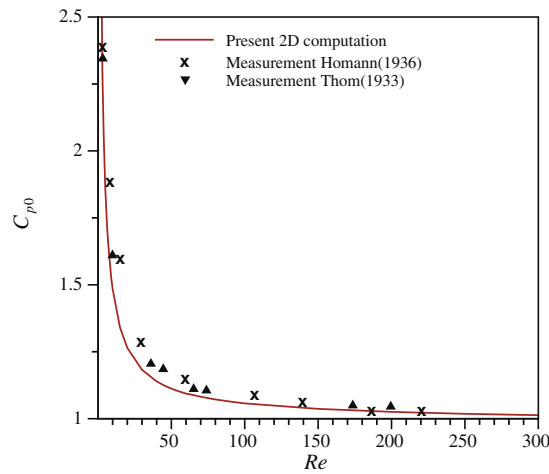


(c) $Re = 300$

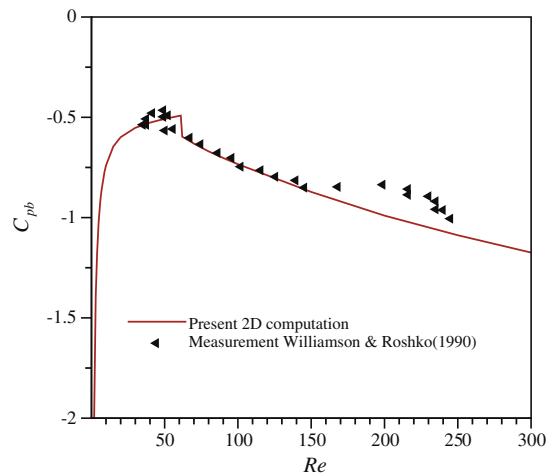
Fig. 4. Surface pressure and skin friction around the cylinder in the periodic laminar regime.



(a) Separation angle



(b) Stagnation pressure C_{p0}



(c) Mean base pressure C_{pb}

Fig. 5. Variation of mean separation angle, stagnation and base pressure with Re .

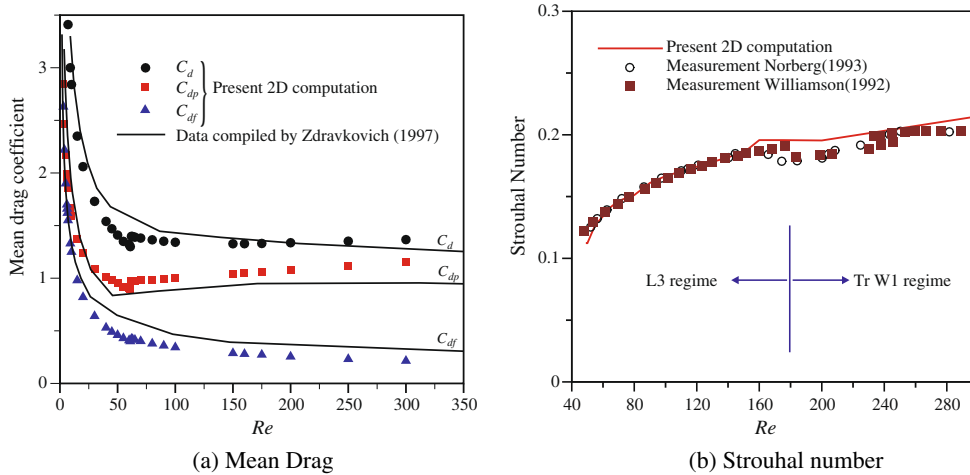


Fig. 6. Variation of mean drag coefficient, Strouhal number with Re .

4.5. Three-dimensional effects on laminar flow past a circular cylinder

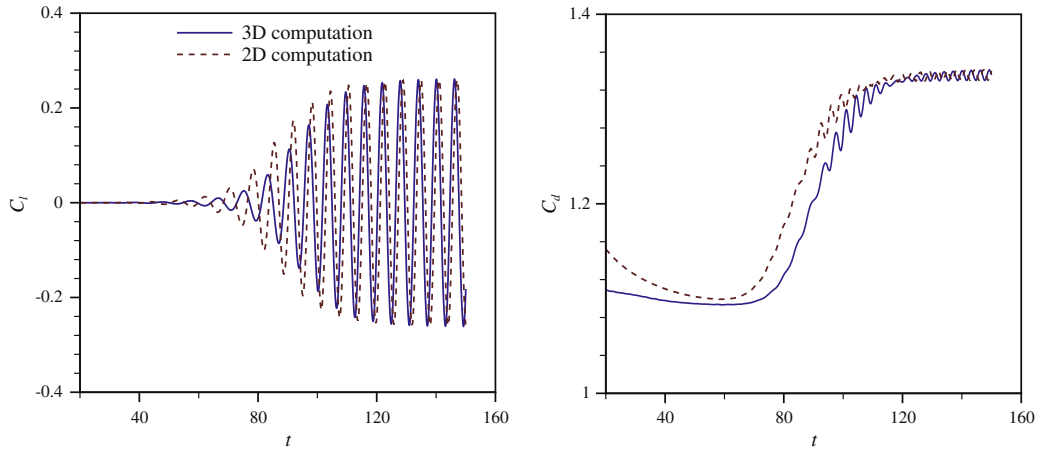
It has been established from the limited measurement and flow visualization studies [25,26] as well as recent direct numerical simulations [27–29] that beyond a certain Reynolds number, the two-dimensional laminar wakes become susceptible to three-dimensional disturbances, when the results of two dimensional flow computation and the derived integrated coefficients for forces and moments on the cylinder become inaccurate. The objective of the present three-dimensional simulation is to investigate whether the present RANS3D code can successfully capture the experimentally observed three-dimensional flow structures beyond a certain Reynolds number and also to confirm whether three-dimensional flow simulations bring more accurate values of the frequency and amplitude of the oscillatory force coefficients. Three-dimensional flow simulations have been carried out for $Re = 100, 200, 250, 300$ and 400 . The present computational domain consists of 32 equidistant parallel planes covering a span length of $2\pi D$, where D is the cylinder diameter and each plane has exactly the same two-block O grid topology (121×144) used in the two-dimensional flow computation. Periodic boundary conditions are used at the end planes along the spanwise direction. The domain span length is chosen following the work of Mittal and Balachandar [8], where the spanwise length of $2\pi D$ is argued to be adequate to cover both the modes of instabilities in the computation.

4.6. Unsteady lift and drag coefficient

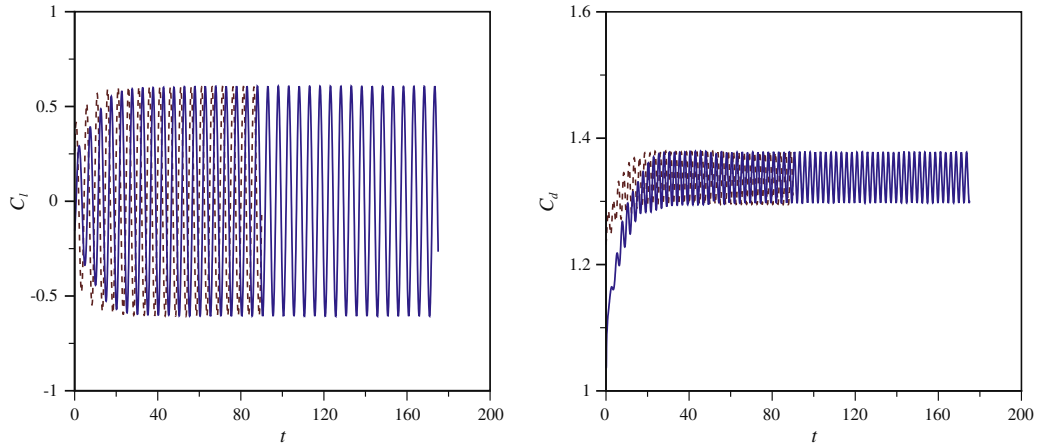
Fig. 7 shows the temporal evolution of the lift and drag coefficients computed separately from both two- and three-dimensional simulation of the flow at all the five Reynolds number between $Re = 100$ and 400 . In all the cases investigated, the initial transients die down in the first few time steps and the flow eventually reaches a periodic but statistically stationary state. The values of Strouhal number, mean C_d and RMS values of C_l , derived from two- and three-dimensional computations are also compared in Table 2. Up to $Re = 200$, the two- and three-dimensional computation results are observed to be almost overlapping, showing no significant difference in the temporal variation of the lift and drag coefficients at the statistically stationary state. As Re increases from 200, the differences observed between the two- and three-dimensional simulation results increase significantly. The magnitude of the maximum lift coefficient and the mean drag coefficient are, in general, observed to be less in the three-dimensional simulation.

Specially at $Re = 300$, where accurate measurement data are available, the Strouhal number and the mean and RMS value of the oscillatory lift and drag forces are evaluated using the Fast Fourier Transform method, from the recorded time history of the corresponding force coefficients. Table 3 compares the present computation results against measurement data and other computation results for the mean base pressure as well as the frequency and RMS amplitude of the aerodynamic force coefficients. The table clearly shows the

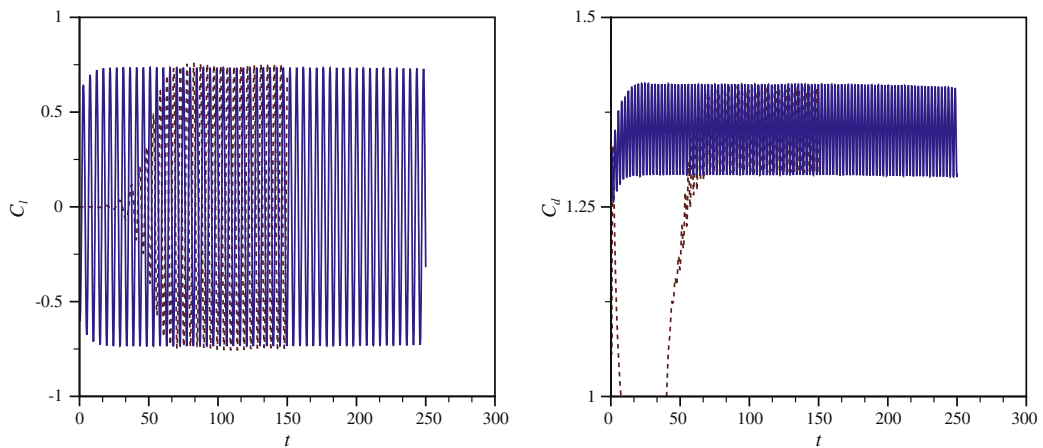
overprediction of the amplitude and frequency of the oscillating force coefficients for two-dimensional simulation of flow at $Re = 300$. Such discrepancies have been explained earlier by Mittal and Balachandar [29] as



(a) $Re = 100$

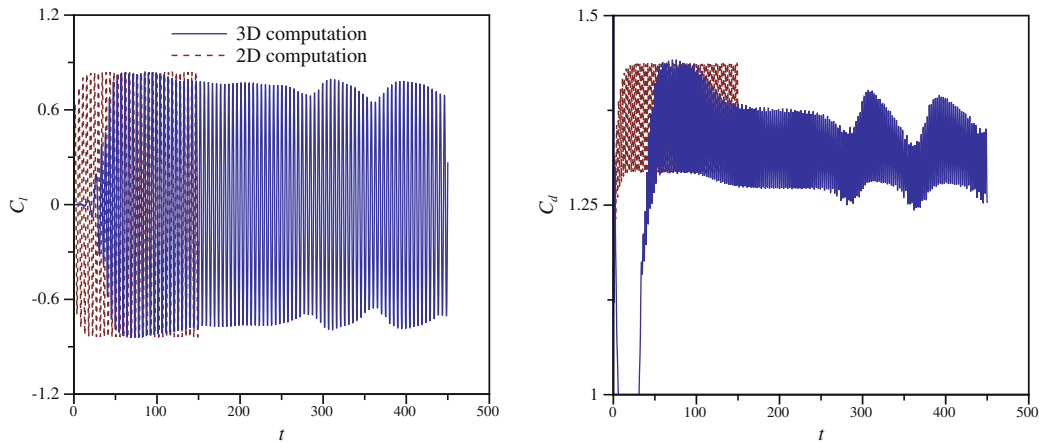


(b) $Re = 200$

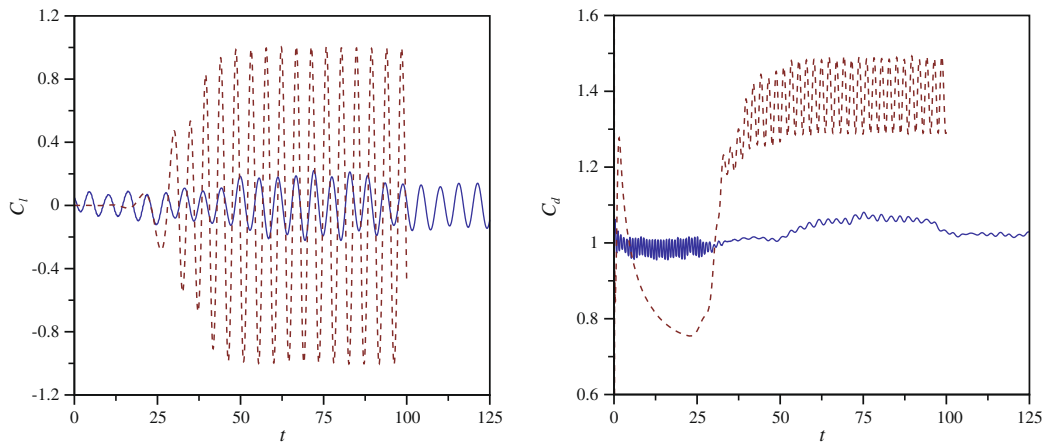


(c) $Re = 250$

Fig. 7. Temporal evolution of lift and drag coefficients for laminar flow past a circular cylinder at different Reynolds number.



(d) $Re = 300$



(e) $Re = 400$

Fig. 7 (continued)

Table 2
Two- and three-dimensional computed Strouhal number, mean drag coefficient and RMS values of lift and drag coefficients

Re	Sr		C_d		C_{lrms}	
	Two-dimensional	Three-dimensional	Two-dimensional	Three-dimensional	Two-dimensional	Three-dimensional
100	0.1569	0.1569	1.3353	1.3349	0.1792	0.1802
200	0.1957	0.1936	1.3365	1.3380	0.4244	0.4276
250	0.2052	0.2100	1.3516	1.3508	0.5283	0.5157
300	0.2150	0.1760	1.3667	1.2840	0.6041	0.5250
400	0.2348	0.1743	1.3905	1.0534	0.7032	0.1295

Table 3
Comparison between computation and measurement for the oscillating forces and base pressure on the cylinder at $Re = 300$

Source of result	Sr	C_{lrms}	C_{davg}	C_{drms}	Mean C_{pb}
Present two-dimensional computation	0.215	0.602	1.37	0.066	-1.17
Present three-dimensional computation	0.195	0.499	1.28	0.067	-1.01
Measurement (Norberg [30])	0.203	0.435			
Measurement (Williamson [6])	0.203				-0.96
Measurement (Wieselsberger [31])			1.22		
Two-dimensional computation (Mittal and Balachandar [8])	0.213	0.650	1.38		-1.22
Three-dimensional computation (Mittal and Balachandar [8])	0.203	0.380	1.26		-0.99

the extraction of energy of the two-dimensional shedding motion by the three-dimensional vortical structures of the flow. This eventually leads to a reduction of the two-dimensional Reynolds stresses which, in turn,

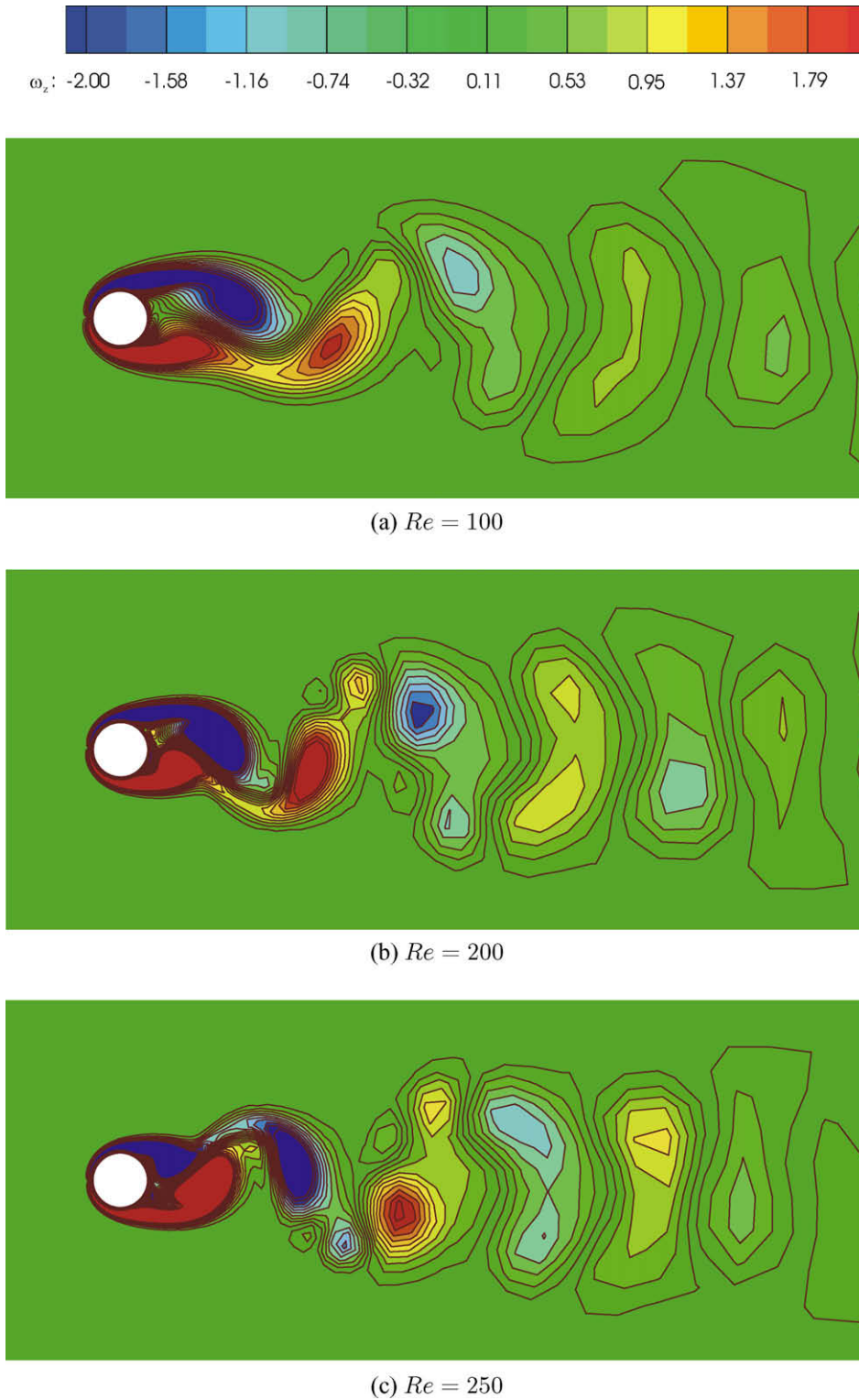


Fig. 8. Instantaneous spanwise vorticity (ω_z) contours on $z/D = 0$ plane for different Reynolds number.

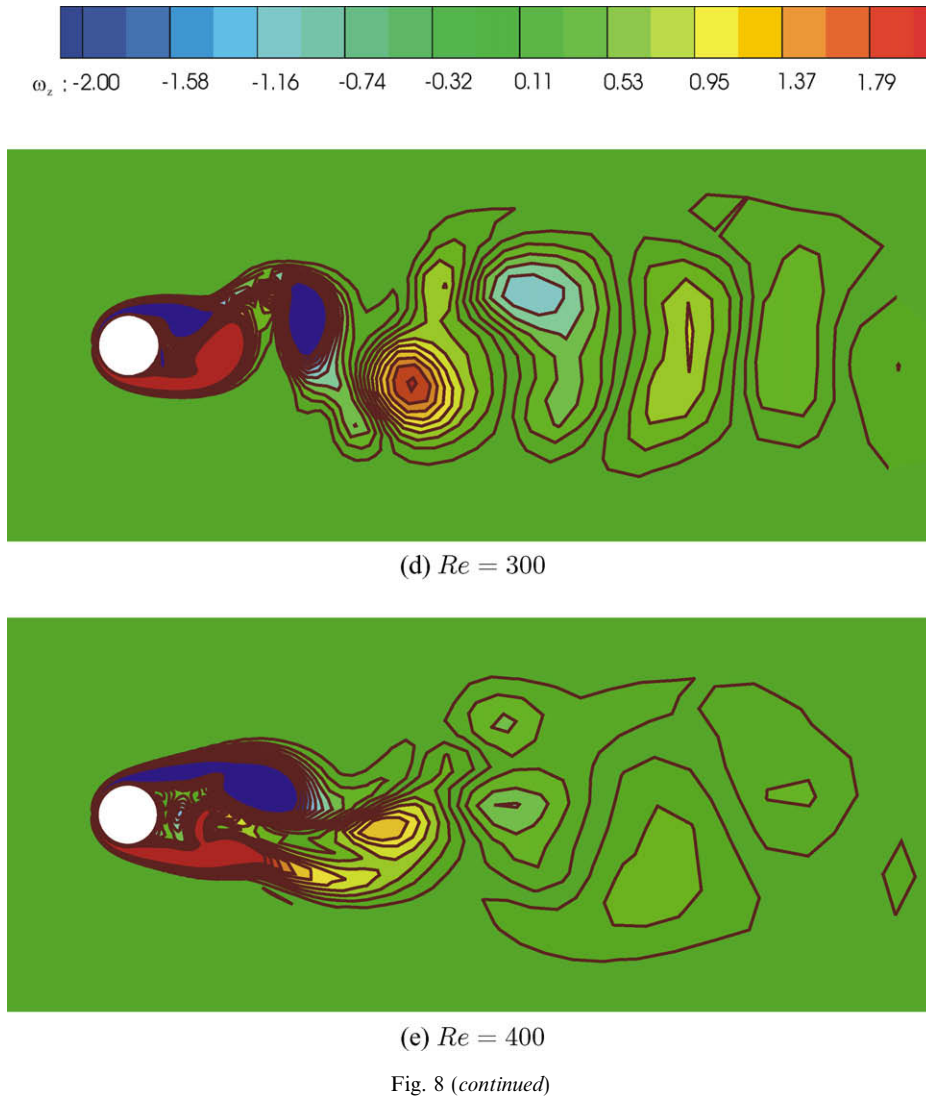


Fig. 8 (continued)

increases the base pressure and hence reduces the mean drag. The table also shows excellent agreement between the measurement data and the present three-dimensional simulations for the mean drag coefficient although the Strouhal number is under predicted by about 4%. However, in case of the best three-dimensional simulation data of Mittal and Balachandar [8] using a longer domain with finer resolution along the span direction, the agreement is excellent for the Strouhal number with a 3% overprediction of the drag coefficient. In spite of the relatively short length of the computation domain and the coarse resolution used along the span direction, reasonably accurate prediction of the unsteady forces has been produced by the Navier–Stokes solver RANS3D for the complex three-dimensional near wake flow behind a circular cylinder at $Re = 300$.

4.7. Flow structure

The laminar flow in the cylinder wake is known [1] to undergo three-dimensional transition instabilities at Reynolds number between 180 and 200. The complex process of viscous diffusion and mutual interaction of laminar eddies shed from the cylinder surface lead to the formation and random growth of irregularities which characterize a finite transition region. However, this transition-in-wake is further subdivided [1] into two flow regimes (i) lower transition regime, (TrW1) when regular laminar eddies are formed which become irregular

and transitional further downstream and (ii) upper transition regime (TrW2) when laminar but irregular eddies are formed which become partly turbulent before they are shed and carried downstream. The recent

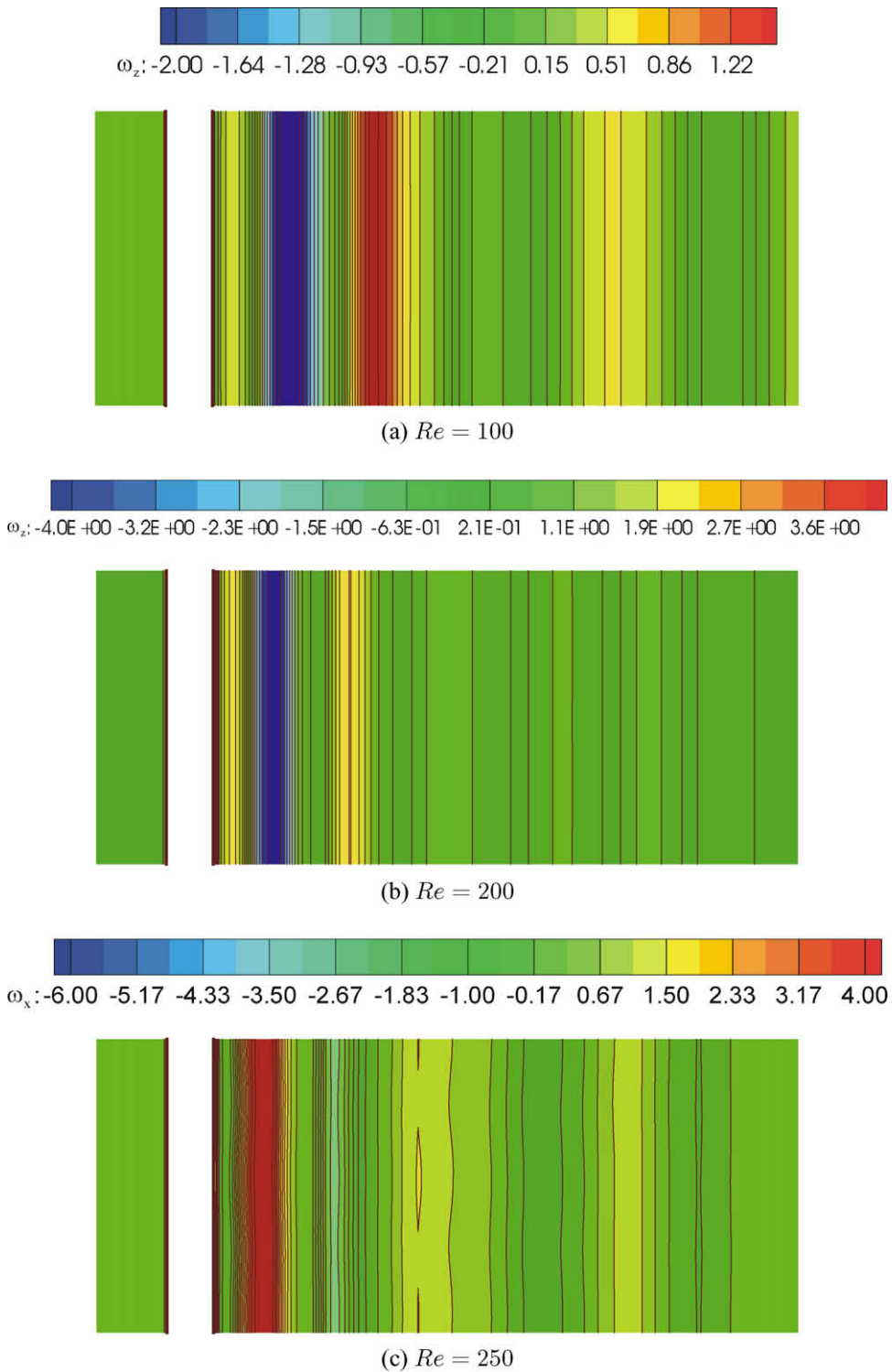


Fig. 9. Instantaneous spanwise vorticity (ω_z) contours on $y/D = 0$ plane for different Reynolds number.

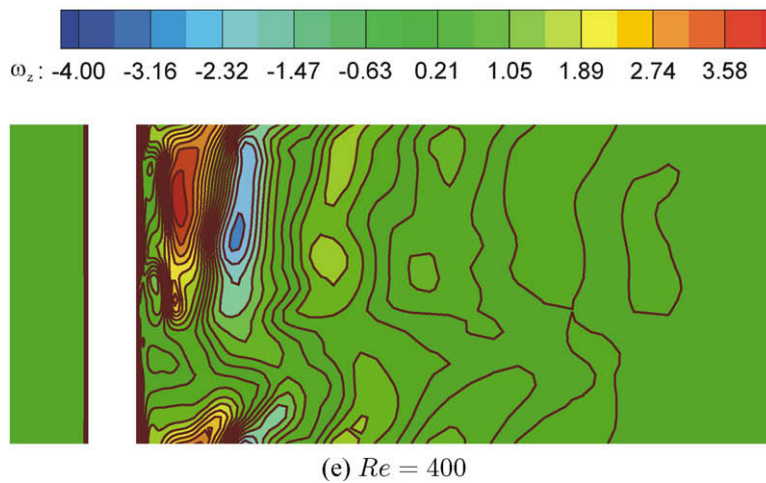
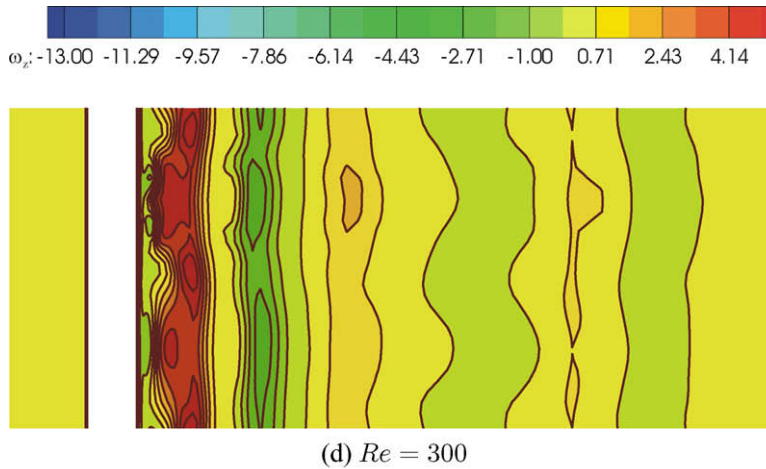
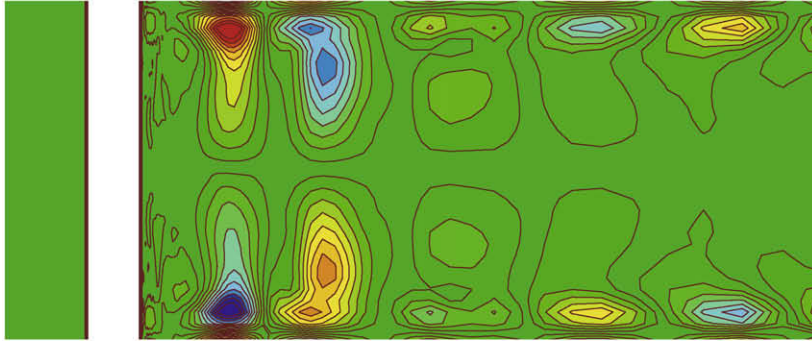


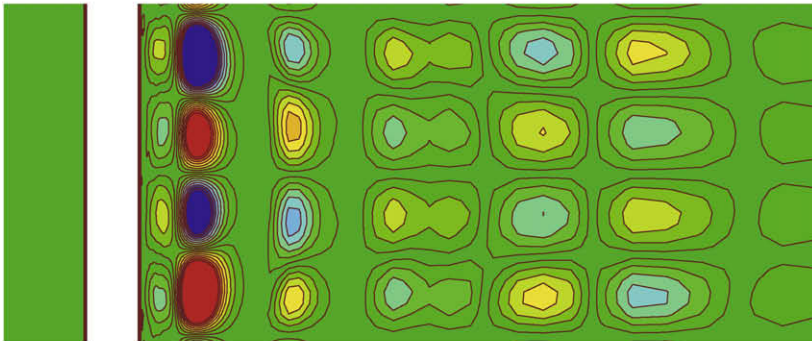
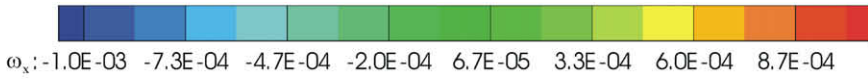
Fig. 9 (continued)

DNS computation of the wake transition at $Re = 300$ by Thompson et al. [7], Zhang et al. [28], Mittal and Balachandar [8] and Mittal [9] have confirmed the existence of such instabilities.

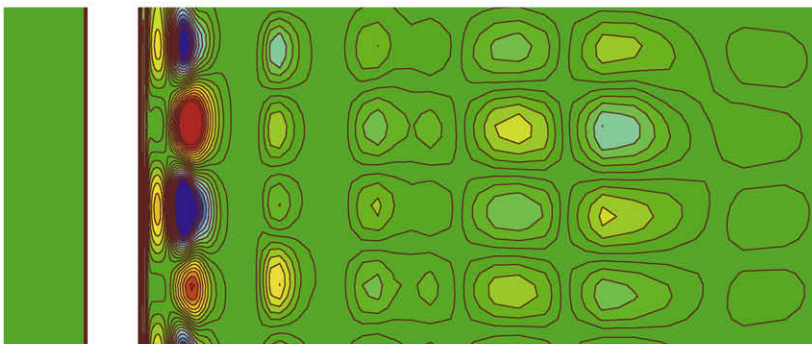
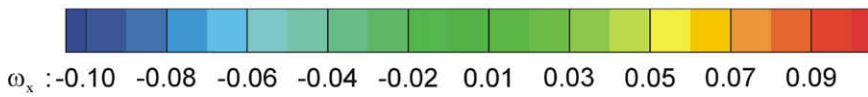
The cylinder wake flow usually consists of different kind of vortical structures which can be conveniently visualized by the contour plots for the vorticity components around the three cartesian axes, which may be easily derived from the computed three-dimensional velocity field at the statistically stationary state of the flow. In the present flow situation, however, the two significant components are the so-called spanwise vorticity component (ω_z) around the cylinder-axis (z -axis) and the streamwise vorticity component (ω_x) around the main freestream flow axis (x -axis). Fig. 8 shows the instantaneous contours of the spanwise vorticity component (ω_z) on a two-dimensional plane ($x - y$) at $z = 0$ for different flow Reynolds number. The value of the vorticity is observed to be varying between -2 and $+2$. The change of sign in the vorticity contours near the cylinder and in the wake clearly shows the phenomenon of alternate vortex shedding. However, for $Re < 300$, the contours are observed to be regular even in the far wake, whereas as Re increases beyond 300 the farwake tends to become irregular. This kind of irregularity of the flow pattern on a typical two-dimensional plane ($z/D = \text{constant}$) may be attributed to the strong three dimensional effects on the dynamics of the flow along the spanwise direction. When the flow is purely two-dimensional, the magnitude of spanwise vorticity should not change along z -direction and hence the ω_z contours on a mid-symmetry plane ($y/D = 0$) are expected to be straight lines parallel to the cylinder axis as observed in Fig. 9a and b for $Re = 100$ and 200. At $Re = 250$ (Fig. 9c) a small lateral distortion of these contours are observed in the far wake and these



(a) $Re = 100$

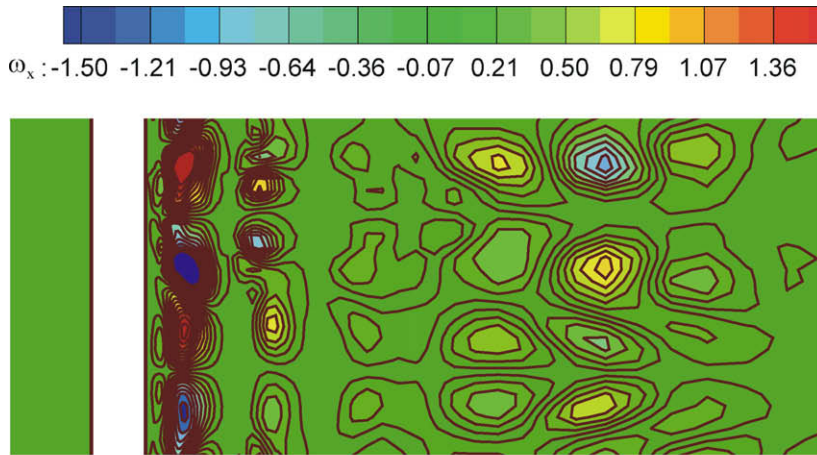


(b) $Re = 200$

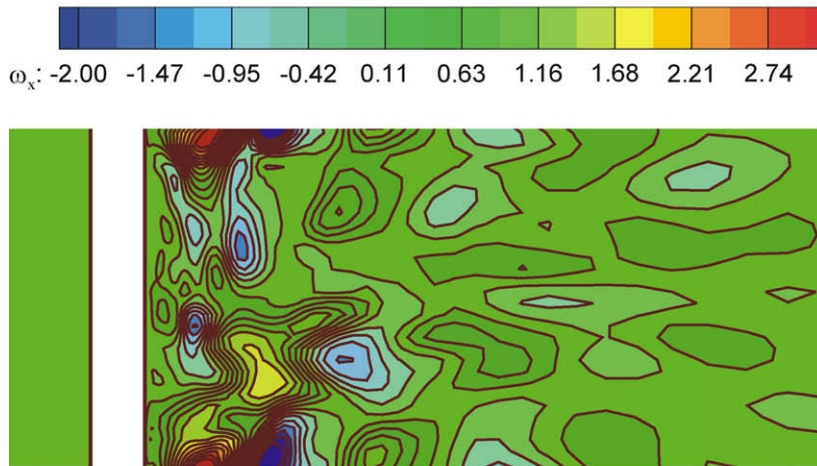


(c) $Re = 250$

Fig. 10. Instantaneous streamwise vorticity (ω_x) contours on $y/D = 0$ plane for different Reynolds number.



(d) $Re = 300$



(e) $Re = 400$

Fig. 10 (continued)

distortions are further enhanced at $Re = 300$ and 400 indicating strong three-dimensional effects. In any three-dimensional flow the effects of cross-flow along a direction normal to the main flow are usually manifested in the form of multiple streamwise vortices around the main flow axis. The vortical structure of the wake flow in the present case may be explained more clearly by looking at the contours of the streamwise vortices (ω_x) on the mid symmetry plane ($y/D = 0$) at different flow Reynolds number. Fig. 10 shows the instantaneous contours of the streamwise vorticity component on the horizontal mid-symmetry plane ($y/D = 0$) at five different Reynolds number. The magnitude of ω_x contour levels for $Re = 100$ and 200 are observed to be very low of the order of 10^{-3} or less which indicate that for $Re \leq 200$ the flow is essentially two-dimensional. However, at $Re = 250$, the magnitude of ω_x level is found to be raised by 100 times (the magnitude is of the order of 0.1 compared to 0.001 for $Re \leq 200$) and such sharp increase in strength of the streamwise vortices clearly demonstrates stronger three-dimensional effects and hence the transition in the wake. But even at $Re = 250$, the formation of the eddies are observed to be quite regular and hence this may be considered to be under the lower transition regime (TrW1) as classified by Zdravkovich 1997 [1]. At and beyond $Re = 300$, the magnitude of ω_x further increases to almost of the order of 2 and the eddies are observed to be quite irregular and hence the flow may be classified under the upper transition regime of the wake (TrW2).

5. Concluding remarks

The wake structure behind a circular cylinder has been computed for both two- and three-dimensional flow, using second order accurate implicit finite volume Navier–Stokes solver RANS3D. Computations have been carried out for Reynolds numbers between 0.1 and 400 covering three different characteristic regimes classified by Zdravkovich [1] – creeping flow (L1), steady closed near wake (L2) and the laminar vortex shedding regime (L3), partly overlapped with the transition-in-wake (TrW) regime. Major physical features of the flow in different regimes are captured by the present computation procedure reasonably well. In the L1 and L2 regimes, reasonably good agreement is obtained between the two-dimensional computation results and the corresponding measurement data for circumferential distribution of surface pressure and skin friction and also for the shape and strength of the steady wake recirculation zone including the separation location. This confirms the adequacy and accuracy of the flow solution algorithm RANS3D. Up to $Re = 200$, the two-dimensional computation results agree reasonably well with the accurate measurement data for the Strouhal number, the base pressure coefficient and the mean drag coefficients. However, beyond the onset of three-dimensional instability at the critical Reynolds number of 180, gross discrepancies have been observed between the two-dimensional flow computation results and measurement data for the Strouhal frequency and amplitude of the fluctuating lift and drag coefficients. The present three-dimensional flow computation has captured all the spanwise as well as streamwise vortical structures of the wake flow, reported in measurement data or other numerical simulations earlier. The computed spanwise and streamwise vorticity component contours viewed on different cartesian planes indicate that the wake structure for $Re > 250$ is less regular with less alignment and shorter wavelength of the streamwise vortices. The prediction of the frequency and amplitude of the fluctuating forces on the cylinder at $Re = 300$ using the present Navier–Stokes solver is also found to be reasonably accurate. Computations are in progress using larger domain and finer resolution along the spanwise direction in order to have a better understanding of the physics of the transition process in the cylinder wake.

Acknowledgements

The authors wish to thank Director NAL Bangalore for his kind permission to publish this paper. Thanks are also due to Dr. Manor T. Nair, Scientist CTFD Division for his valuable suggestions and advice at different stages of this work.

References

- [1] M. Zdravkovich, *Flow Around Circular Cylinders*, vol. 1, Oxford Science Publication, 1997.
- [2] S. Majumdar, W. Rodi, J. Zhu, Three-dimensional finite volume method for incompressible flows with complex boundaries, *J. Fluid Eng. ASME* (1992) 496–503.
- [3] S. Majumdar, Pressure based Navier–Stokes solver for three-dimensional flow in hydrodynamics and low speed aerodynamics application, in: *Proceedings of the 3rd Asian CFD Conference*, Bangalore, vol. 1, 1998, pp. 137–146.
- [4] S. Majumdar, B.N. Rajani, Numerical computation of flow around aerostats using a pressure-based Navier–Stokes solver, *J. Aeronaut. Soc. India* 53 (2) (2001) 117–127.
- [5] S. Majumdar, B.N. Rajani, D.S.Kulkarni, S.Mohan. RANS computation of low speed turbulent flow in complex configuration, in: *Proceedings of the Symposium on State of the Art and Future Trends of CFD at NAL*, NAL SP03 01, 2003, pp. 31–48.
- [6] C.H.K. Williamson, Vortex dynamics in the cylinder wakes, *Ann. Rev. Fluid Mech.* 28 (1996) 477–539.
- [7] M. Thompson, K. Hourigan, J. Sheridan, Three-dimensional instabilities in the wake of a circular cylinder, *Exp. Thermal Fluid Sci.* 12 (1996) 190–196.
- [8] R. Mittal, S. Balachandar, On the inclusion of three-dimensional effects in simulation of two-dimensional bluff-body wake flows, *ASME Fluids Engineering Division Summer Meeting*, 1997.
- [9] S. Mittal, Computation of three-dimensional flow past circular cylinder of low aspect ratio, *Phys. Fluids* 13 (2001) 177–191.
- [10] S.V. Patankar, *Numerical Heat Transfer and Fluid Flow*, Hemisphere Pub., Co., 1980.
- [11] P.K. Khosla, S.G. Rubin, A diagonally dominant second-order accurate implicit scheme, *Comput. Fluids* 2 (1974) 207–209.
- [12] H.L. Stone, Iterative solution of implicit approximations of multidimensional partial differential equations, *SIAM J. Numer. Anal.* 5 (1968) 530.
- [13] D.D. Barkley, R.D. Henderson, Three-dimensional Floquet stability analysis of the wake a circular cylinder, *J. Fluid Mech.* (1996).
- [14] B.N. Rajani, Harsha Gopal Lanka, S. Majumdar. Laminar flow past a circular cylinder at Reynolds number varying from 50 to 5000, NAL PD CF 0501, 2005.

- [15] S. Manoj Kumar, Numerical Computation of Turbulent Flow Past Bluff Bodies, M.Tech Thesis, Department of Mechanical Engineering, National Institute of Technology, Calicut, Kerala, 2004.
- [16] S. Taneda, Experimental investigation of the wakes behind cylinder and plates at low Reynolds number, *J. Phys. Soc. Jpn.* 14 (1956) 843.
- [17] M. Coutanceau, R. Bouard, Experimental determination of the main features of the viscous flow in the wake of a circular cylinder in uniform translation: steady flow, *J. Fluid Mech.* 70 (1977) 231.
- [18] F. Homann, Influence of higher viscosity on flow around cylinder, *Forsch. Gebiete Ingenieur.* 17 (1936) 1–10 (in German).
- [19] C. Norberg, An experimental investigation of the flow around a circular cylinder: influence of aspect ratio, *J. Fluid Mech.* 258 (1994) 287.
- [20] B. Kumar, S. Mittal, Prediction of the critical Reynolds number for flow past a circular cylinder, *Comput. Meth. Appl. Mech. Eng.* 195 (2005) 6046–6058.
- [21] H.G. Dimopoulos, T.J. Hanratty, Velocity gradients at the wall for flow around a cylinder for Reynolds number between 60 and 360, *J. Fluid Mech.* 33 (1968) 303–319.
- [22] A. Thom, The flow past circular cylinder at low speeds, *Proc. Royal Soc. A* 141 (1933) 651–669.
- [23] C.H.K. Williamson, A. Roshko, Measurement of base pressure in the wake of a cylinder at low Reynolds numbers, *Zeits. Flugwiss. Weltraum.* 14 (1990) 38–46.
- [24] C. Norberg, Pressure forces on a circular cylinder in cross flow, in: H. Eckelmann, J.M. R. Graham, P. Huerre, P.A. Monkewitz (Eds.), *Bluff-Body Wakes Dynamics and Instabilities*, Springer-Verlag, Berlin, 1993, pp. 275–278.
- [25] F.R. Hama, Three-dimensional vortex pattern behind a circular cylinder, *J. Aeronaut. Sci.* 24 (1957) 156.
- [26] J.H. Gerrard, The wakes of cylindrical bluff bodies at low Reynolds number, *Philos. Trans. Royal Soc., Lond. Ser. A* 288 (1978) 351.
- [27] G.E. Karniadakis, G.E. Triantafyllou, Three-dimensional dynamics and transition to turbulence in the wake of bluff objects, *J. Fluid Mech.* 238 (1992) 1–30.
- [28] H.Q. Zhang, U. Fey, B.R. Noack, M. König, H. Eckelmann, On the transition of the cylinder wake, *Phys. Fluids* 7 (1995) 779–794.
- [29] R. Mittal, S. Balachandar, Generation of streamwise vortical structures in bluff body wakes, *Phys. Rev. Lett* 75 (5) (1995) 1300–1303.
- [30] C. Norberg, Flow around circular cylinder: aspects of fluctuating lift, *J. Fluid Struct.* 15 (2001) 459–469.
- [31] C. Wieselsberger, New data on the law of hydro and aerodynamic resistance. NACA TN 84, 1922 (in German).